RECENT RESULTS BY THE UNIVERSITY OF FLORIDA GROUP FROM LOW FREQUENCY RADIO OBSERVATIONS OF JUPITER AND NEPTUNE

T. D. Carr*, K. Imai†, L. Wang‡, L. Garcia*,
F. Reyes*, C. H. Higgins*, and W. B. Greenman*

Abstract

We summarize results from research projects conducted by the University of Florida Low Frequency Radio Astronomy Group during the past two years. Not included here are two of the projects that are covered in the two succeeding papers in these proceedings, by Higgins et al. and Reyes et al. We start with a brief summary of an already published paper on the successful modeling of the emission beam shape and source location for Neptune's smooth radio component as observed by Voyager 2. We then summarize a new paper (JGR, in press) on our multielement interference grating model for the production of Jovian decametric modulation lanes, after which we suggest a much simpler and far more plausible two-path interference model that would produce an interference pattern having the same fringe separation as would the multielement grating. Some of the unpublished results of an extensive investigation of long term periodicities in 37 years of Florida Jovian decametric observational data are presented, with emphasis on the effects of the variation in D_E on Earth-observed Non-Io-A emission. Finally, a previously unpublished method is presented for obtaining Jovian S burst intensity vs. time and frequency vs. time information with unprecedented resolution (down to 3 μsec). Initial results are included that are believed to provide for the first time information on individual highly localized cyclotron maser wave amplification events.

1 Introduction

In this paper and in two others [Higgins et al; Reyes et al., this volume] we present some of the more interesting results, either unpublished or published within the past two years,

*Department of Astronomy, University of Florida, Gainesville, FL 32611, USA
†Departm. of Electrical Engineering, Kochi National College of Techn., Nankoku, Kochi 783, JAPAN
‡Applied Research Corporation, Landover, MD 20785, USA

that have been obtained largely from decametric observations of Jupiter at the University of Florida Radio Observatory and from Voyager observations of Neptune. The paper by Higgins et al. [this volume] is a report on our new measurement of the rotation period of Jupiter's inner magnetosphere. Reyes et al. [this volume] summarizes the results of coordinated decametric monitoring of Jupiter during the impacts of fragments of Comet S-L 9 by our group and others from several world-wide locations.

During the past two years, PhD degrees have been awarded to three members of our low frequency radio astronomy group, their dissertations contributing to the results presented here. The references for the three dissertations, and papers subsequently published that were based mainly on the dissertation results, are:
(1) Dissertation: Wang [1994]; papers: Wang and Carr [1994]; Wang and Carr [1995].
(2) Dissertation: Higgins [1996]; paper: Higgins et al. [1996].
(3) Dissertation: Garcia [1996].

References to other papers that have been published within the past two years by our group, or are in the process of publication, are Carr et al. [1994]; Carr et al. [1995]; and Imai et al. [1997]. Some results from four of the recent research projects by our group are discussed in this paper.

2 Neptune's smooth radio component

Wang and Carr [1995] investigated the principal smooth component of Neptune's hectometric-kilometric radio emission, as recorded by Voyager 2. A geometric model for the source distribution and emission beam was developed for that part of the smooth emission component in the frequency range between 40 and 400 kHz. At each frequency, the model parameters were adjusted to provide a best fit of the calculated intensity vs. time curve to the observed intensity vs. time curve. Assumptions made in developing the model were (1) Neptune's magnetic field distribution is that of the O_8 model of Connerney et al. [1991], (2) the radio source at a given frequency is so distributed that X mode emission toward the spacecraft would be RH elliptically polarized, (3) the resultant beam is composed of elementary hollow cone beam components for which the cone axes are tangent to the magnetic field at the individual source elements (all the cone half-angles being equal) (4) all the source elements for a given emission frequency lie just above the surface on which the electron cyclotron frequency equals that frequency, and (5) all ray paths to the spacecraft lie entirely outside this surface.

It was found that the source area was of sufficiently limited extent that the resultant beam from the entire source, as well as the beam from each source element, is in the form of a hollow cone. The sources of radiation at the three widely separated frequencies 116, 251, and 404 kHz were found to lie mostly within 20° of the north magnetic pole, overlapping about half of the northern auroral zone indicated by Connerney et al. [1991]. Ladreiter et al. [1991] had previously developed a model for the same radio source based on the earlier (and oversimplified) offset dipole magnetic field model. Their indicated source region was an arc-shaped area well outside the north auroral zone but partially surrounding it, at a distance of about 55° from the north magnetic pole. The discrepancy between the source

locations of Ladreiter et al. [1991] and Wang and Carr [1995] is probably largely due to differences in the magnetic field models used.

Other results deduced from the modeling were:
(1) The half-angle of the resultant hollow cone beam was about 80°.
(2) There is evidence that the source was located within a plasma-depleted cavity.
(3) At 116 kHz (but only near that frequency) a probable O mode component was identified in addition to the usual X mode component.

3 Jovian decametric modulation lanes

Jupiter's modulation lanes, the sloping increased-intensity bands sometimes appearing in dynamic spectra of Jovian decametric activity, were discovered by Riihimaa [1968, 1970]. He has provided most of the available observational information on this interesting phenomenon (see, e.g., Riihimaa [1993]). He showed that when a suitable multi-slotted "screening structure" moves across a decametric source area being observed from Earth, a dynamic spectrum closely resembling modulation lanes could be produced. He suggested that such a structure might be located at a distance of about 50 Jovian radii from the source, perhaps at the magnetospheric boundary [Riihimaa, 1971, 1974]. On the other hand, Imai et al. [1992a, 1992b] have presented compelling evidence supporting the idea that modulation lanes are a wave interference phenomenon rather than one resulting from a simple screening of the source, and that the interference-producing elements are located near Io's orbit close to the longitude of the Sub-Earth Point. Imai et al. assumed that the interference pattern is produced by scattered radiation from a planar multielement grating consisting of nearly equally spaced field-aligned columns of slightly enhanced (or depleted) plasma. The model was adjusted to fit the observational data remarkably well. Although no satisfactory explanation has been given for the occurrence of such an unlikely grating structure, it appears probable that no other location for *any* type of interference-producing plasma structure than one near Io's orbit close to the longitude of the Sub-Earth point can provide a fit to the observations. It should be noted that the geometry for the production of sloping dynamic spectral modulation lanes by our interference grating is essentially the same as that proposed by Riihimaa for his "screening structure".

Using unpublished data kindly provided by Dr. Riihimaa, together with data obtained with the 640-dipole 26.3 MHz array of the University of Florida, Imai, Wang, and Carr have extended the results previously obtained with their modulation lane model. A paper based on these new results has been accepted for publication in *J. Geophys. Res.* The results include the following: (1) Further confirmation that the Io-B and Io-A radiations are emitted from the northern hemisphere, while that from Io-C comes mainly from the southern hemisphere (the latter being a new result). (2) The half-angle of the assumed hollow-cone emission beam for Io-B is 60°, with a variation of only a few degrees. (3) Modulation lanes from Io-unrelated emission were successfully modeled. (4) The depth of modulation was measured with considerable precision for both Io-B and Io-A lanes, and was found to be much less for Io-A than for Io-B.

Imai et al. [1992a, 1992b, and 1997] have thus presented most convincing evidence that

Jovian modulation lanes are indeed an interference phenomenon produced by some type of field aligned plasma structure located near Io's orbit close to the longitude of the Sub-Earth Point. It is much less certain, however, that this interference-producing structure is their proposed multi-column grating. The probability of the existence of such a plasma structure in Jupiter's magnetosphere appears to be vanishingly small. There are other much simpler and more probable plasma structures that could be made the basis for the model, and would lead to the same results as have been obtained by Imai et al.

Perhaps the most attractive alternative model, in its simplest form, is based on a single field-aligned column or curtain of enhanced plasma density that resulted from a volcanic eruption by Io. After the discharged gas cloud becomes ionized, subsequent diffusion is constrained to the field lines within its flux tube; hence its initial alignment with the field (later it will also spread across the field due to such effects as grad-B drift and curvature drift). Let us consider the propagation of rays emitted from a small source near the northern foot of the flux tube previously energized by Io. We consider only those rays lying within a plane nearly perpendicular to the magnetic field lines that contains the observer on Earth. The rays passing through different parts of the plasma column (or curtain) are refracted by different amounts. It is therefore not improbable for a ray to be refracted by the small angle necessary to render it parallel to the ray that is headed directly for Earth. It can be shown that the required amount of this refraction is less than a half minute of arc, an amount that should be easily obtainable. When received at Earth, the two rays will have traveled over different path lengths and will thus produce a quasi-sinusoidal interference pattern. We refer to this process as two-path interference.

The direct ray path lies well outside the column. We represent its distance of closest approach to the favorably refracting part of the column by d. It can easily be shown that if R is the distance of the column from the radio source, λ is the wavelength, and n is the order of a resulting interference fringe maximum observed at Earth, the following approximate relation holds:

$$d = \sqrt{2n\lambda R} \tag{1}$$

For both the grating model and the two-path interference model, the angular separation between successive fringe maxima at a given frequency would be approximately λ/d radians (where d in the case of the grating is the column spacing). The shape of the intensity vs. time curve for a fringe of a given order, however, would be different in the two cases. Instead of being quasi-sinusoidal as in the two-path model, each fringe peak for the grating model would be narrower. Its angular width would be approximately $\lambda/(Nd)$ radians, where N is the number of scattering columns in the grating.

If the single-column two-path model is assumed, it seems likely that there would often be two or more such columns at different distances from the direct ray, each contributing (in conjunction with the direct ray) its own two-path interference pattern. In this case the single frequency fringe pattern would be more complex than the sinusoidal pattern obtained with a single-column. This would seem to be in agreement with observed modulation lanes; while their single-frequency intensity variation may tend to be sinusoidal for short intervals, the complexity of the pattern is not inconsistent with the possibility of the

superposition of two or more slightly different two-path interference patterns. Another factor contributing to the observed complexity, if the two-path model is assumed, would be the time variations in the structure of the refracting column. And of course for any model, interplanetary scintillation would profoundly modulate the interference pattern on a time scale that is usually somewhat longer than that of the fringe periodicity.

Thus far we have discussed the interference patterns only at a single frequency. Actually, a band of frequencies is emitted simultaneously, the sources of the individual frequencies being at different heights within the flux tube that was previously energized by Io (the highest frequency being at the least height, and vice versa). These component sources will also be located at slightly different longitudes because of the tilt of the flux tube with respect to the meridian planes intersecting it. The interference patterns for the individual frequency components are thus relatively displaced in longitude. Due to this effect together with Jupiter's rotation, a given fringe maximum (i.e., one of a given order, n) that is observed at Earth at one frequency and time will progress to higher (or lower) frequencies at later times. This is the explanation of the slopes of the modulation lanes in recordings of the dynamic spectrum. Since these fringe slopes and spacings would be the same for the simplest two-path interference model as for the simplest grating model, essentially the same results that have been obtained by *Imai et al.* with the grating model would also be obtained with the proposed two-path model. We plan to investigate the two-path model further by making ray tracings through assumed field-aligned columns having different cross sectional shapes and radial plasma density distributions.

4 Long-term periodicities in the Jovian decametric radiation

4.1 The 37–year data set

Using the data set accumulated from 37 years of observations of Jovian decametric radiation by the Florida group, Garcia, in collaboration with Carr and Reyes, is making a thorough investigation of known and suspected periodicities in both the occurrence probability per apparition and the averaged flux density (actually the occurrence probability weighted by flux density) per apparition. The longest series of observations were made at the three frequencies 18, 20, and 22.2 MHz, using separate tracking 5-element yagi antennas or their equivalent. A shorter series has been made at 26.3 MHz with the 640-element phase-steered antenna array. The identifiable "sources", Io-B, Io-A, Io-C, Non-Io-A, and Non-Io-C, as well as the total radiation from all source regions, were investigated separately. In addition, this unprecedentedly extensive data set is being used to redetermine the boundaries of the above source regions on the Io phase vs. CML plane, and to study the Jovian *elongation effect*.

4.2 Known periodicities

Although there has yet been no positive identification of any periodicity in the actual emission of decametric radiation from Jupiter that is causally related to some other periodic phenomenon, several pronounced periodicities are observed in the emissions that

are received at Earth or at a spacecraft. The best known of these, which are due to periodicities in the times during which the observer is well inside an emission beam, are (1) The 9.92 hour period of Jupiter's rotation, which causes the variation of observed occurrence probability with CML; (2) the 1.77 day period of the orbital motion of Io, which is responsible for Io's control of observed occurrence probability; and the 11.9 year period of Jupiter's orbital motion, which causes the observed variations with respect to D_E.

A significant correlation with respect to the 30-day smoothed sunspot number, the average period of which is about 10 or 11 years (depending on the averaging interval), has been sought unsuccessfully since shortly after the discovery of the radiation. Because of the masking effect of the powerful 11.9-year periodicities related to Jupiter's orbital motion, it has not yet been shown that there is a true correlation with sunspot number (after discounting the effects due to the terrestrial ionosphere). If a true correlation were established, it might be attributed to some effect of either the solar wind or the solar ultraviolet radiation on the plasma in the radio emission region, or alternatively, to an increase in scattering loss with respect to the sunspot number-correlated increase in electron density as the radiation propagates through the interplanetary medium.

We are using the 37-year data set to investigate all the above-mentioned periodicities, and wherever possible to establish (or to improve on) a quantitative relationship between the appropriately averaged decametric occurrence probability and the other periodic phenomenon with which it is correlated. This is very difficult to accomplish, except of course for the case of the already intensively investigated periodicities due Jupiter's rotation and Io's orbital motion. For example, the 37 years of observations must have been made with equipment and observing procedures that have remained sufficiently unchanged that the data can be considered uniform in that respect. In the data reduction process, all radio interference must be identified and properly and consistently taken into account, calibrations must be applied, and realistic corrections must be made for uncontrollable factors such as changes in galactic background temperature. We summarize some of the results that have thus far been obtained.

4.3 Non-Io-B

Non-Io-B activity at the sensitivity levels attainable with the 5-element yagi antennas used in this study is rare. The active CML source regions at these sensitivities are Io-B, Io-A, Non-Io-A, and Io-C. After the first apparition of Jovian observations with the Florida 640-dipole 26.3 MHz array, however, the great increase in sensitivity revealed a Non-Io-B source of high activity but relatively low flux density [Desch et al., 1975]. So far as we know, there has been no confirmation of this result. We therefore have analyzed the large-array data obtained during the seven apparitions following the one of the Desch et al. result. The earlier results are fully substantiated. The average flux density of Non-Io-B bursts appears to be about a factor of ten less than that of Io-B, but its occurrence probability is comparable to that of Io-B. We will obtain quantitative estimates of the long-term average occurrence probabilities and flux densities of the five sources Io-B, Non-Io-B, Io-A, Non-Io-A, and Io-C in the 18 to 26.3 MHz spectral region.

4.4 New observations of D_E effects

Carr et al. [1970] showed from 18 MHz observations made over one cycle of D_E variation that three parameters of source A (i.e., Io-A and Non-Io-A combined) that are strongly correlated with the mean D_E value for an apparition are (1) the CML of the center of the source A peak on the histogram of occurrence probability vs. CML for an apparition, (2) the occurrence probability per apparition, and (3) the effective width of the source A peak, in terms of CML. Gulkis and Carr [1966] had previously discovered (1) above, and concluded that it is a consequence of the geometrical relationship between the observer and the source A emission beam. Carr et al. [1970] concluded that (2) and (3) are also effects of this geometry.

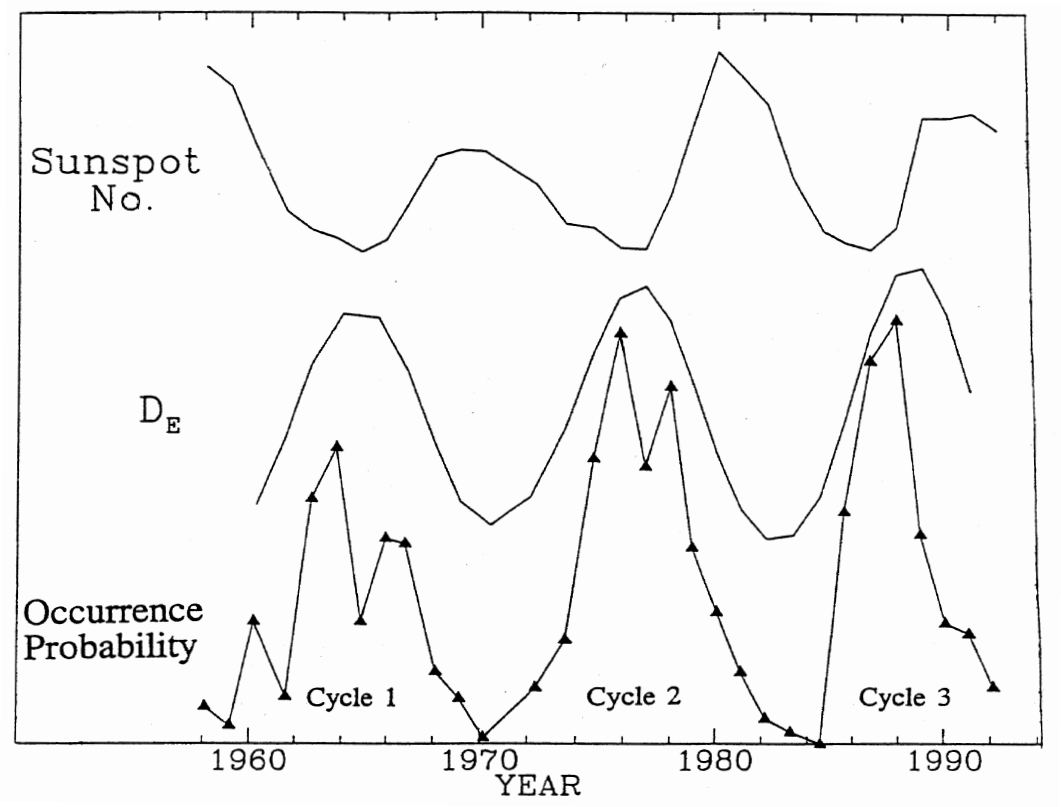

Figure 1: Comparison of the shapes of the time variations of the apparition-averaged sunspot number, the apparition-averaged value of D_E, and the Non-Io-A occurrence probability per apparition.

Garcia has included a re-investigation of (2) and (3) above in his analysis of 37 years of decametric data (except that he studied Io-A and Non-Io-A separately instead of combined). He has investigated the time variation of both occurrence probability per apparition and averaged flux density per apparition at 18, 20, and 22.2 MHz, for each of the sources Io-B, Io-A, Non-Io-A, and Io-C. In every case, the predominant periodicity is that of D_E. The correlation with D_E is more pronounced in the case of the curves of occurrence probability than with those of average flux density, the latter being subject to larger erratic fluctuations. The source that exhibits the highest correlation with D_E is Non-Io-A. Figure 1 is

a comparison, for three 11.9-year D_E cycles, of the shapes of the time variations of the apparition-averaged sunspot number, of the apparition-averaged value of D_E, and of the 18 MHz Non-Io-A occurrence probability per apparition. The apparent anticorrelation of sunspot number with D_E is of course coincidental and temporary, but it has been troublesome. It has thus far made it impossible to ascertain definitely whether there is some degree of true negative correlation of occurrence probability with sunspot number as well as the dominant positive correlation with D_E. We believe that the notch in the peak that occurs in the occurrence probability curves near the times of highest D_E for both Cycles 1 and 2 is a real effect. The notch in the Cycle 2 curve has previously been found to be present in three independent data sets—those of the Universities of Florida, Chile, and Colorado (see St. Cyr [1985]).

4.5 Empirical modeling of the Non-Io-A D_E effect

We have developed an empirical model for the time variation of occurrence probability per apparition for Non-Io-A at 18 MHz. It was assumed that the occurrence probability (P) for each of the three D_E cycles is proportional to the product of two functions. The first is $p(D_E)$, the component of the occurrence probability variation due to the D_E variation alone. The second, p(SSN), is assumed to be a probability component that is due to the variation in sunspot number alone. The constant of proportionality (K) that provided the best fit to the observed curve was determined separately for each of the three cycles. Thus

$$P = K[p(D_E)][p(SSN)] \tag{2}$$

Figure 2a shows the best fitting function $p(D_E)$ for Cycles 1 and 2; Figure 2b shows that for Cycle 3. Figure 2c shows the function assumed for the sunspot number variation for all three cycles. The best fitting values of K for the three cycles were 0.21, 0.39, and 0.28, respectively. The modeled and observed curves are plotted together in Figure 2d. The fit, while far from perfect, is probably as close as could be expected considering the inevitable errors incurred in determining occurrence probability. The notches at the peaks of Cycles 1 and 2 were generated by the assumed steep decrease in $p(D_E)$ with increasing D_E when the latter is greater than 2.4°. For the modeling of Cycle 3, however, which displayed no such dip, it was necessary to assume an increase in $p(D_E)$ over the entire D_E range.

The inclusion of the p(SSN) factor for an assumed anticorrleation of occurrence probability with sunspot number improved the fit somewhat over what it would have been for no assumed sunspot number control at all. It contributed to a slight extent to the sharp decline in occurrence probability that started at the expected location of the Cycle 3 notch. However, this improvement was not great enough that we can state unequivocally that solar activity really does influence the occurrence probability. It appears that the old question whether there is a solar activity effect as well as the D_E effect must remain unanswered for a few more years, until the time variations of D_E and sunspot number separate further from their near-antiphase relationship that has prevailed since the discovery of the Jovian decametric radiation.

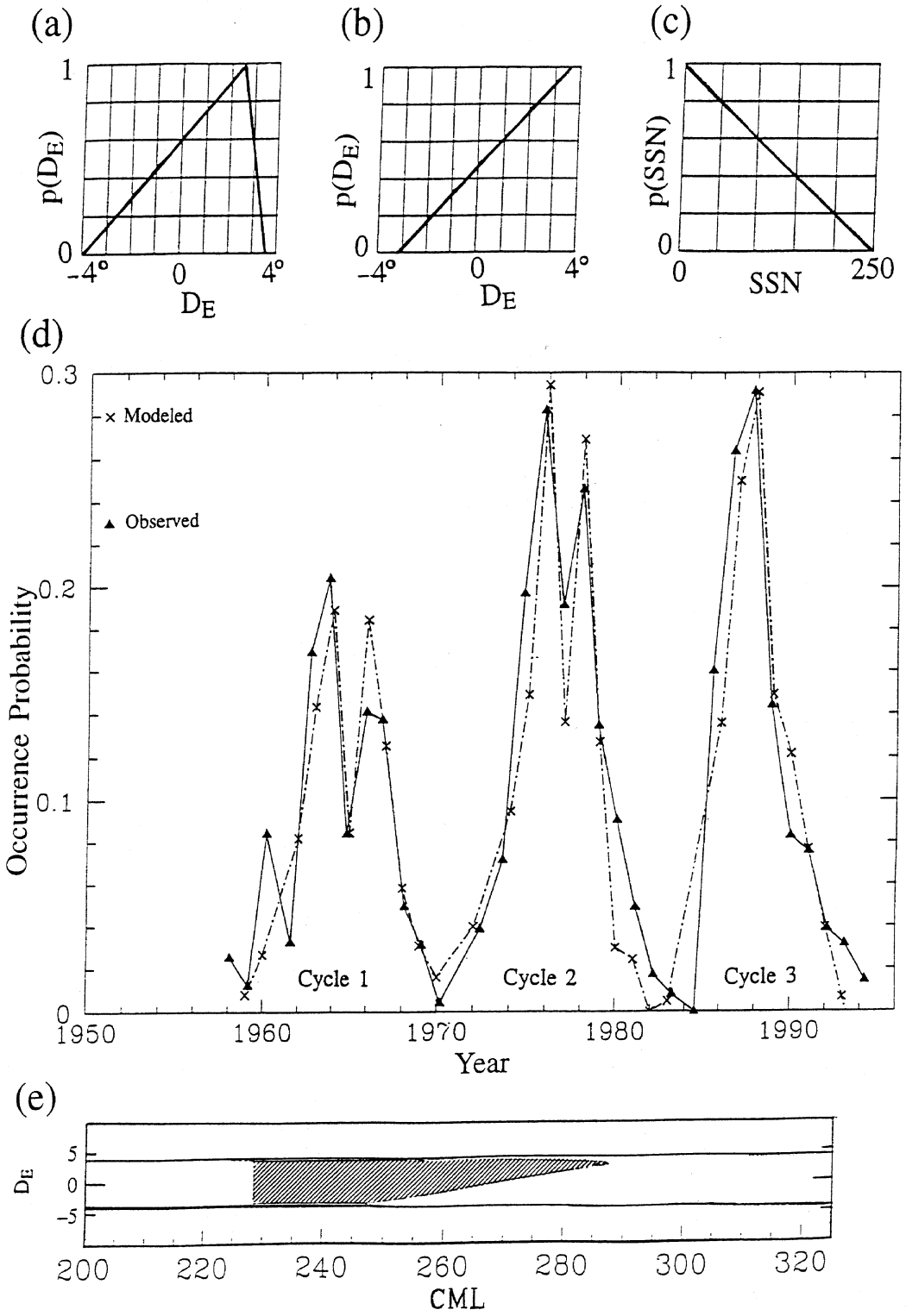

Figure 2: a) Assumed D_E variation of the occurrence probability component controlled by D_E alone, for Cycles 1 and 2. b) Same for Cycle 3. c) Postulated occurrence probability component controlled by sunspot number alone, for all three cycles. d) Comparison of the resulting modeled occurrence probability vs. time curve with the observed curve. e) Observed distribution of Non-Io-A activity on the D_E vs. CML plane (hatched area).

4.6 Variation of the width of the Non-Io-A occurrence probability vs. CML peak with D_E

Carr et al. [1970] found from the data obtained from a single 11.9-year cycle of D_E that on plots of occurrence probability per apparition vs. CML, the *width* of the source A peak varies markedly with the median value of D_E per apparition. Most of this source width variation occurred at the high-CML edge of source A. The low-CML edge remained nearly constant. We have repeated such an investigation, measuring for each apparition the CML values at the low-CML and high-CML edges of source Non-Io-A (instead of source A as Carr et al. did; source A includes Io-A as well as Non-Io-A), and using the data from about three D_E cycles (actually 37 years). Our new results fully substantiate the earlier conclusions of Carr et al. [1970]. The hatched area in Figure 2e represents the Non-Io-A activity distribution on the D_E vs. CML plane, as determined from our 37 years of observations. It can be seen that the low-CML edge is vertical and the high-CML edge has a very pronounced slope, as found in the earlier measurements.

The hatched area in Figure 2e can be interpreted as the cross section of that part of the Non-Io-A emission beam that is observable at Earth. The beam rotates with Jupiter. Most of the beam lies in the inaccessible area above the $D_E = 3.3°$ line. Earth just happens to be direction of the extreme bottom part of this beam. The fact that a decrease of only 5° in D_E can cause such an extreme reduction in source width indicates that (1) Earth is in the direction of the bottom part of this beam, being below nearly all of the beam when D_E is at its most negative value, (2) the lower boundary of the beam is amazingly sharp and stable. This interpretation suggests that the observed variation of Non-Io-A occurrence probability per apparition is due simply to the fact that, generally, less of the beam is observable from Earth on each Jovian rotation the lower is the value of D_E. We tested this hypothesis by assuming the $p(D_E)$ is proportional to source width as a function of D_E. We were then able to derive from the observed variation in source width a curve of $p(D_E)$ vs. D_E that closely resembles that in Figure 2a over most of the D_E range. We are thus confident that it is indeed the variation of the amount of the rotating beam that can be observed from Earth that causes the variation of occurrence probability with D_E. We are attempting to determine the origin of this most unusual beam.

5 Measurement and interpretation of the finest observable S burst structure

5.1 Dynamic spectra of simple S bursts

The dynamic spectra of typical Jovian S bursts of the simplest type, as received with the 640-dipole 25.8-to-26.8 MHz antenna array at the University of Florida Radio Observatory and a baseband-output receiver having a bandwidth of 500 kHz, are illustrated in the top panel of Figure 3. Similar illustrations of the dynamic spectra of a large number of S bursts of this type, and of other types, can be seen in the S-burst catalog by Flagg et al. [1991]. Each simple S burst observed in this part of the spectrum decreases in frequency,

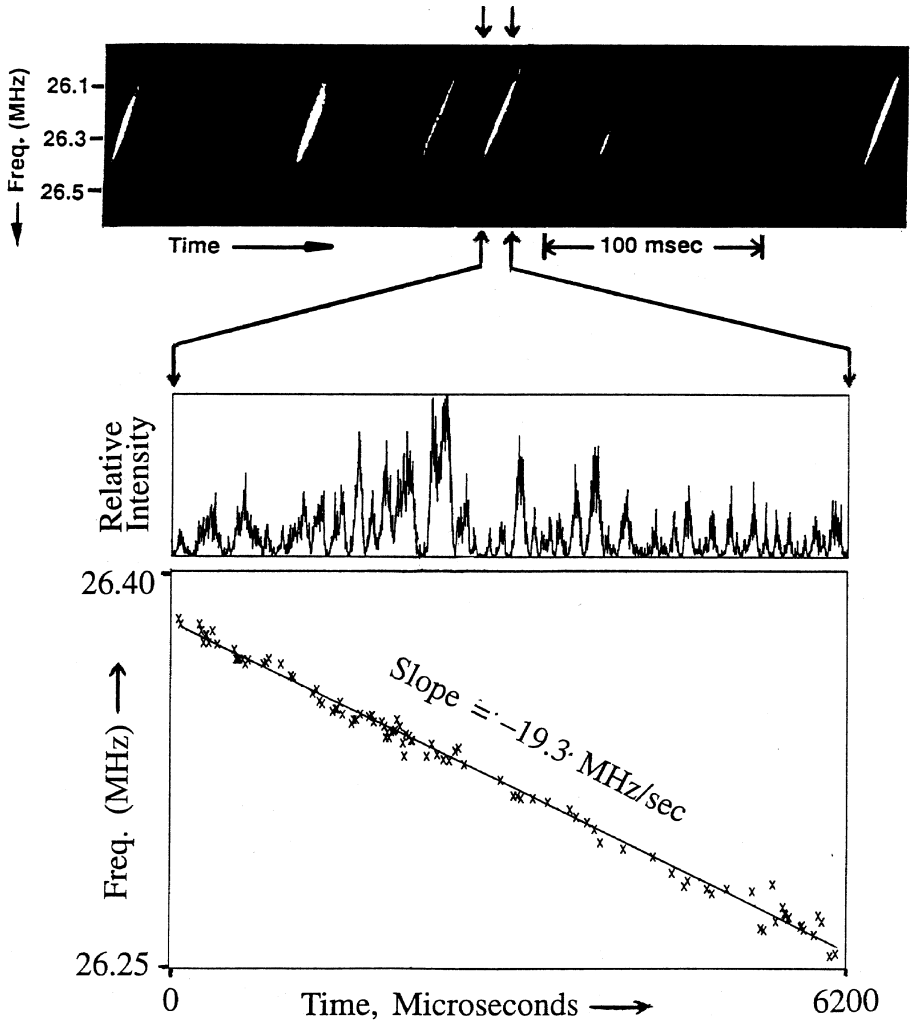

Figure 3: Upper panel; Simple S bursts. Middle Panel; Intensity vs. time curve, to a greatly expanded time scale, for the S burst located between the arrows in the upper panel. Lower panel; Measured points of the S burst frequency vs. time, with a least-squares line fit to the points.

without exception, at a drift rate of about −20 MHz/sec. We have examined the intensity-time and frequency-time structure of the particular S burst indicated between the arrows in Figure 3, using progressivly increasing resolution. The duration of this S burst was 6.2 milliseconds (msec). We were able to observe its structure on time scales down to a few microseconds (μsec), approaching the shortest time scale at which significant structure can exist. It should be noted that there were only about 26 oscillations per μsec at the receiver input due to the S burst, and that the dynamic spectral structure resides in the time-varying power spectrum resulting from the *modulation envelope* of these radio frequency (RF) oscillations.

5.2 Achieving higher time resolution

The dynamic spectrum illustrated in the top panel of Figure 3 was obtained with a spectrograph capable of a time resolution of about 300 μsec. We now briefly describe our new method for reducing this resolution limit, for the special case of simple S bursts, by as much as two orders of magnitude. Our well-known procedure for obtaining spectra of the type shown in the top panel of Figure 3 involves the analog recording of the receiver baseband output with a tape recorder having a tape speed of 120 inches/sec, and subsequently processing the signal played back at a tape speed of about 1 inch/sec (see Flagg et al. [1991]). This system has been used at the University of Florida Radio Observatory for many years. The first step of our new method is to digitize the voltage from the played-back taped signal at such a rate as to provide one sample every 0.31 μsec of real (original) time. This corresponds to one new sample over the time required by every 8 RF oscillations at 26.3 MHz.

5.3 Intensity and frequency vs. time with 30 μsec resolution

It is now a simple matter to compute the S burst intensity vs. time curve for any desired time resolution greater than about 3 μsec. This is done by simulating a *square-law detector*. The digitized S burst voltage oscillations are first adjusted to have a long-time average value of zero by subtracting the initial value of the long-time average from each individual value. Each of these individual background-subtracted voltages is then squared, and the resulting values are *low-pass filtered* with a filter having a cutoff frequency for which the period is the desired limit of time resolution. In practice, this filtering is accomplished by taking the running average over a sliding interval having a duration of 3 μsec or more, depending on the resolution limit that is wanted (the process is also known as "boxcar" averaging or smoothing). This method provided the intensity vs. time curve shown in the middle panel of Figure 3 for our selected 6.2 msec S burst. The smoothing interval used here was about 30 μsec. The pulsed structure that is displayed in this panel has not previously been observed, so far as we are aware. These irregular pulses are about 200 μsec apart, on the average. We suggest that they result from the modulation of the S burst emission process by some type of plasma oscillation at the source.

To obtain a curve of S burst frequency vs. time with the same resolution as was used above, we measured the mean frequency of the digitized S burst over fixed and irregularly spaced smoothing intervals of about 30 μsec each. Each such measurement was accomplished by first multiplying (in the computer, not electronically) a time segment of the background-subtracted S burst signal by a sinusoidal function of adjustable frequency which we refer to as the *local oscillator* frequency, appropriately smoothing the product over the duration of the time segment. Then the local oscillator frequency was re-adjusted and the process repeated until zero-beat with the S burst signal was obtained. This frequency equals the mean value of the S burst frequency, averaged over the duration of the smoothing interval. The resulting frequency vs. time plot for the 6.2 msec duration of the selected S burst is shown in the bottom panel of Figure 3. The fluctuations of the individual frequency measurements about the least-squares line are definitely not due to measurement error–

they are true fluctuations, of physical origin, in the actual frequency values. The slope of the line, representing the mean frequency drift rate, is −19.3 MHz/sec.

5.4 Calculation of the velocity of the source region along the Io flux tube

The drift rate measurement provides a means for measuring the upward velocity of the source region within the Jovian magnetic field. The S burst occurred during a typical Io-B storm. We make the usual assumption that the radiation is emitted within the northern arm of the Io flux tube (IFT) at a frequency slightly higher than the electron cyclotron frequency, f_c, at the source location. The approximation is made that the emitted frequency *equals* f_c. Let r be the measured mean frequency drift rate (which is negative) over the entire 6.2 msec S burst in Figure 3. Let s be the distance upward along the IFT from the cloud-top level to the region of emission. The velocity of the latter is $v = \frac{ds}{dt}$. At this location, $\frac{df_c}{ds} = 2.8\frac{dB}{ds}$, where B is the magnetic field strength, in gauss, and f_c is in MHz. But since $r = \frac{df_c}{dt} = \frac{df_c}{ds}\frac{ds}{dt}$, we have $r = 2.8v\frac{dB}{ds}$. The velocity can thus be calculated from

$$v = r/(2.8\frac{dB}{ds}) \tag{3}$$

Using the value of r as determined from the slope of the straight line fit in Figure 3, together with the value of $\frac{dB}{ds}$ as calculated from the O_8 field model, we obtain $v = 16400$ km/sec for the upward velocity of the region of emission along the IFT.

5.5 Highest resolution measurements

We now refine the method of frequency measurement in order to obtain significant values with a time resolution of a few microseconds. The new procedure involves the following steps: (1) The relative phase, δ, of the local oscillator as well as its frequency, F, are made adjustable; (2) the computer calculates the mean intensity (averaged over each smoothing interval, as was done above) as a function of time; (3) the computer calculates the mean phase difference, ϕ, between the S burst oscillation and the local oscillator signal (averaged over each smoothing interval) as a function of time; and (4) the computer calculates the correlation coefficient between the S burst oscillation and the local oscillator signal (averaged over each smoothing interval) as a function of time. In each step boxcar smoothing over a 3 μsec sliding interval was employed.

We illustrate in Figure 4 the type of result obtained by this method. We have chosen for this example a 200 μsec segment enclosing the largest of the pulses appearing in the middle panel of Figure 3. This part of the relative intensity vs. time curve is reproduced, to an expanded time scale, in the top panel of Figure 4. Below it in the figure are nine square panels, arranged in three columns and three rows. In each column, the three panels contain plots of intensity vs. time, phase difference ϕ vs. time, and correlation coefficient vs. time. Each column represents a case for which it has been possible to make adjustments of the frequency F of the local oscillator until a flat section of the ϕ vs.

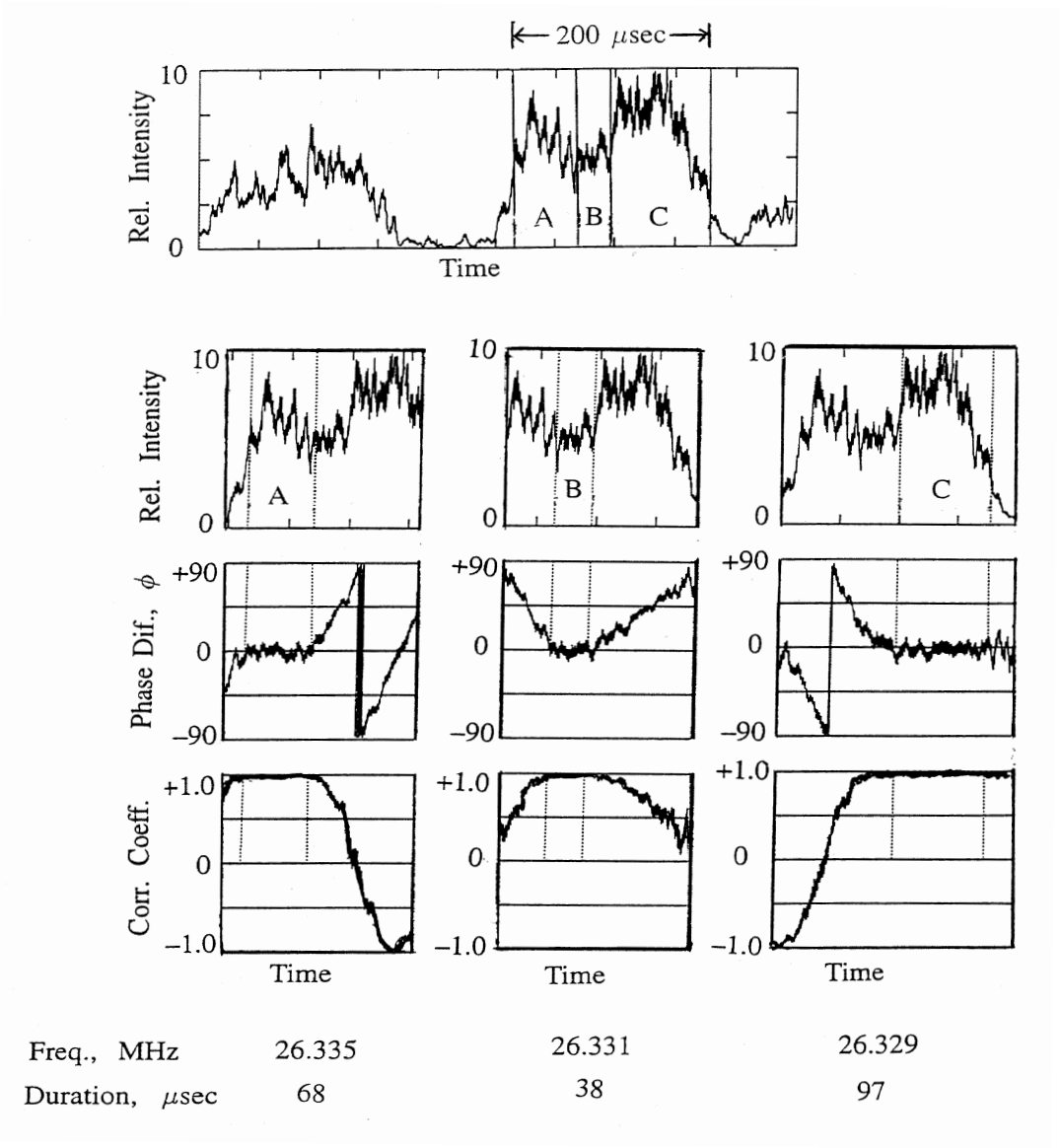

Figure 4: Upper panel; Intensity vs. time curve for two of the largest pulses appearing in the middle panel of Figure 3. First column of 3 square panels, from top to bottom; Intensity, phase difference between S burst and the local oscillator, and correlation coefficient, respectively, vs. time, when the local oscillator has been set to 26.335 MHz, at a particular phase (the interval A between vertical dotted lines is 68 μsec). Second column of 3 square panels; Same except that frequency has been set to 26.331 MHz at a new phase (the interval B is 38 μsec). Third column of 3 square panels; Same except that the frequency is now 26.329 Mhz, at a readjusted phase (interval C is 97 μsec).

time curve appears, and then to adjust the relative phase, δ, of the local oscillator (with slight readjustments of F) until the flat section has been moved up or down to the $\phi = 0$ axis. Thus in the first column, F has been adjusted to 26.335 MHz (real-time equivalent RF frequency) and δ has been adjusted to some particular value (not indicated) that caused ϕ (in the middle panel) to remain near zero for about 68 μsec. At the end of this 68 μsec interval, the ϕ vs. time curve abruptly started to rise at an angle of about

45°. It can also be seen, from the bottom panel, that over the same 68 μsec interval the correlation coefficient remained close to 1.0, but suddenly started decreasing at the end of the interval. Thus the local oscillator signal matched the S burst signal in both frequency and phase for the 68 μsec interval, but not for times before or after that. The S burst signal was thus nearly monochromatic for that length of time. This interval is labeled A.

The next such interval over which ϕ could be made to remain near zero for an appreciable time was B, in the second column. Here the adjustment of F to 26.331 MHz and δ to some particular value (different from the previous one) caused ϕ to remain at approximately zero for 38 μsec. The next quasi-monochromatic interval is C in the third column. It is the longest, lasting for 97 μsec. Its frequency was 26.329 MHz. It is apparent that for these three intervals, the S burst frequency decreased in discrete steps, rather than decreasing smoothly. It can also be noted in the panel at the top of Figure 4 that there are significant differences in the intensity vs. time curve for segments A, B, and C, as well as the differences in frequency and phase.

5.6 Interpretation of the results

We have already suggested, as have others previously, that the observed negative drift rates of S bursts result from the motion of the emitting electrons upward along the IFT into regions of progressively lower f_c. We have calculated their component of velocity parallel to the magnetic field to be 16400 km/sec. The kinetic energy associated with this parallel velocity component is about 0.8 keV. Since the emitting electrons have just mirrored, the kinetic energy associated with the perpendicular velocity component must be considerably greater than this. It therefore appears not unlikely that the electron total energy is in the vicinity of 5 or 10 keV.

We have suggested that the intensity pulses, i.e., those with separations of about 200 μsec in the middle panel of Figure 3 and the upper panel of Figure 4, are the result of the modulation of the source by some sort of plasma oscillation. We suggest one of the possible methods by which such a modulation might take place. It is well known that for the cyclotron maser to operate, the ratio of the plasma frequency (f_p) to the electron cyclotron frequency must be less than a certain small quantity ϵ, that is,

$$\frac{f_p}{f_c} < \epsilon \tag{4}$$

The quantity ϵ has most often been assumed to be about 0.1, but it is now believed to be much smaller than this (J.D. Menietti, private communication). We therefore suggest that it is the density maxima of the plasma oscillation that periodically shut off the cyclotron maser, because then $\frac{f_p}{f_c} > \epsilon$, while the density minima of the oscillation allow the maser to operate because then $\frac{f_p}{f_c} < \epsilon$. Assuming that the wavelength of the oscillating plasma is relatively long, we can conclude that the period of the plasma oscillation is approximately 200 μsec, i.e., the approximate mean period of the observed intensity pulses. The corresponding frequency is 5 kHz. It might therefore be concluded that f_p and ϵ are on the order of 5 kHz, and 0.0002, respectively.

We now offer an explanation of our observation that the S burst frequency decreases in small irregular steps instead of decreasing smoothly with time. To be included in the explanation is the fact that three such well defined quasi-monochromatic steps as A, B, and C can occur within a single intensity pulse like the one analyzed in Figure 4. It is reasonable to start by assuming that the sources of the individual quasi-monochromatic emission steps, which we designate *subsources*, are at different *fixed* locations along the path of the upward-streaming electrons. Each subsource location is fixed in the magnetic field at a place at which f_c is approximately the observed emission frequency of that subsource. Each subsource emits its radiation only when a certain segment of the ascending electron stream passes it. This segment, which we refer to this as the *active segment*, is a limited region of the ascending electron stream within which conditions for the onset of the cyclotron maser instability are favorable. It is this active segment that is ascending the IFT at the velocity $v = 16400$ km/sec.

The location of a particular subsource relative to the magnetic field is simply the point at which the wave amplification accompanying a particular cyclotron maser instability event happened to begin. Once the emission process has started, however, that subsource remains fixed relative to the magnetic field as it emits at a nearly constant frequency. Emission terminates when the wave amplification process can no longer be sustained. According to our measurements, this occurs after an emission period of up to a few tens of μsec duration. Very often there is only one subsource emitting at a time, as was true throughout the intensity pulse containing A, B, and C in Figure 4. We can easily recognize when two or more subsources are emitting simultaneously, for then it is impossible to make ϕ (see Figure 4) remain near zero and the correlation coefficient cannot be brought close to 1.0, regardless of the local oscillator settings F and δ.

The frequencies of successive subsource emission events generally decrease, but not uniformly. There is considerable scatter in the successive values. The tendency for the frequencies to decrease is of course due to the passage of the active segment into regions of ever-decreasing magnetic field strength. The scatter indicates that successive subsources are turned on at slightly different points within in the frame of the smoothly ascending active segment of the electron stream. The pronounced tendency for each new subsource, at its slightly different (usually lower) frequency, to become activated immediately upon the termination of the previous one, as is beautifully illustrated by A, B, and C in Figure 4, must now be explained.

At this point we offer a qualitative (and far from complete) description of the situation at a time of wave amplification at a particular subsource, at a particular frequency, due to the cyclotron maser instability. The upward streaming electrons, gyrating about a tube of magnetic flux f_c times per second, possess a loss-cone pitch angle distribution as a consequence of having just mirrored. Partial phase-bunching of the electrons has taken place–electrons have become concentrated within one half of each distance of a complete gyration and depleted in the other half. There are thus electric (E) field vectors directed from the direction of the electron depletion regions toward the electron concentration regions. The vectors rotate about fixed points on the axis of the flux tube as the gyrating electron stream passes by. The relative rotational phases of the successive E vectors along the axis are such that an electromagnetic wave is continually being launched. The wave

propagates outward and forward within a hollow-cone beam that is coaxial with the flux tube. The half-angle of the hollow-cone beam at 26.3 MHz is about 70° [Maeda and Carr, 1992]. Each wavefront (corresponding to a certain phase value) is also conical, but its surface slants backward rather than forward. The wavenormal at each point of each wavefront is at an angle of about 70° from the outward direction of the flux tube axis. For as long as the proper phase relation between the gyrating electron bunches and the electromagnetic wave prevails, energy from the electrons is fed into the wave, amplifying it, and at the same time the electrons are kept sufficiently well bunched by the wave. But this phase relation does not remain constant. After the gyrating electron bunches and the electromagnetic wave have drifted sufficiently far apart in phase, the cyclotron maser stops operating. This is supposedly what caused the abrupt termination of each of our many well defined quasi-monochromatic emission events within a few tens of μsec after its commencement. We assume that as the termination time approaches at the currently active subsource, the phase relationship at the next site downstream to become active may be rapidly improving. Thus the transition time between the death of one subsource and the birth of the next may be very short, as is illustrated in Figure 4.

Whether or not our interpretation is correct, our revelation of detailed intensity-time and frequency-time S burst structure on time scales extending from the previously attainable 300 μsec down to about 3 μsec provides a new type of diagnostic probe for the investigation of individual highly localized cyclotron maser amplification events. We have observed many clearly defined quasi-monochromatic events having durations between 10 and 100 μsec. The distances traveled by the upward- moving stream of gyrating electons during these time intervals range from 0.2 to 1.6 km. We therefore believe that the dimensions of the cyclotron maser subsources responsible for such brief emission events are less than, say, 1.6 km. A new window has been opened for making investigations of such small scale events in the Jovian magnetosphere.

Acknowledgements: This work was supported in part by *National Science Foundation* Grant AST 94-06501 and by *National Aeronautical and Space Administration* Grant NAGW-2410.